Paleoceanography and Paleoclimatology

RESEARCH ARTICLE
10.1029/2023PA004677

Key Points:

- We present quantitative estimates of Plio-Pleistocene North African monsoon activity based on deconvolution of planktonic foraminiferal $\delta^{18}O$
- Through the past 5 million years estimated monsoon activity is consistent with the expected pattern of orbital eccentricity modulation
- Apparent monsoon strengthening at ~2.6 Ma may be due to shifting runoff sources induced by Northern Hemisphere ice sheet initiation

Supporting Information:

Supporting Information may be found in the online version of this article.

Correspondence to:

D. Heslop,
david.heslop@anu.edu.au

Citation:

Heslop, D., Amarathunga, U., & Rohling, E. J. (2023). Estimating Plio-Pleistocene North African monsoon runoff into the Mediterranean Sea and temperature impacts. *Paleoceanography and Paleoclimatology*, *38*, e2023PA004677. https://doi.org/10.1029/2023PA004677

Received 8 MAY 2023
Accepted 19 OCT 2023

Author Contributions:

Conceptualization: D. Heslop, U. Amarathunga, E. J. Rohling
Formal analysis: D. Heslop, U. Amarathunga
Methodology: D. Heslop, E. J. Rohling
Software: D. Heslop
Validation: D. Heslop, U. Amarathunga, E. J. Rohling
Writing – original draft: D. Heslop, U. Amarathunga, E. J. Rohling
Writing – review & editing: D. Heslop, U. Amarathunga, E. J. Rohling

© 2023 The Authors.
This is an open access article under the terms of the Creative Commons Attribution-NonCommercial License, which permits use, distribution and reproduction in any medium, provided the original work is properly cited and is not used for commercial purposes.

Estimating Plio-Pleistocene North African Monsoon Runoff Into the Mediterranean Sea and Temperature Impacts

D. Heslop[1], U. Amarathunga[1,2], and E. J. Rohling[1,3]

[1]Research School of Earth Sciences, Australian National University, Canberra, ACT, Australia, [2]Department of Geosciences, Princeton University, Princeton, NJ, USA, [3]Ocean and Earth Science, National Oceanography Centre, University of Southampton, Southampton, UK

Abstract Sapropels are dark, organic-rich layers found in Mediterranean sediments that formed during periods of bottom water anoxia. While various mechanisms have been proposed to have caused anoxic conditions, a primary factor is considered to be water column stratification induced by freshwater runoff related to intensified North African monsoon precipitation during precession minima. Monsoon intensification also induced Green Sahara Periods that may have impacted North African hominin dispersal. In this study, we present a novel regression-based deconvolution of a high-resolution planktonic foraminiferal oxygen isotope record to estimate the combination of freshwater runoff reaching the eastern Mediterranean and associated surface warming of the water column over the past 5 million years. Sapropels are known to occur in clusters associated with periods of high orbital eccentricity. Our analysis reveals a consistent influence of orbital eccentricity in modulating the North African monsoon, and a possible shift in runoff source area induced by the initiation of Northern Hemisphere ice sheets. Our findings provide important insights into the role of the North African monsoon in shaping Mediterranean environmental changes over the past 5 million years.

Plain Language Summary We investigate long-term changes in monsoon rains over North Africa, which annually result in freshwater flowing into the Mediterranean Sea. Over geological time, Earth's orbital variations have played a significant role in shaping the monsoon and, consequently, the quantity of freshwater entering the Mediterranean. Foraminifera, small marine organisms, record the oxygen isotope composition of their environment in their shells. Notably, the oxygen isotope balance in North African monsoon rains and the Mediterranean Sea differ, but eventually mix upon the freshwater entering into the Mediterranean. Our research combines a statistical analysis of oxygen isotope data preserved in foraminifera shells with a numerical model of the Mediterranean Sea, enabling us to estimate changes in monsoon freshwater input into the Mediterranean over the past 5 million years. This information not only enhances our understanding of monsoon evolution but also provides insights into the potential for hominin migrations in a more lush North African landscape characterized by higher rainfall than today.

1. Introduction

Intercalated marls and organic-rich sapropel layers in sedimentary sequences have provided crucial insights into the evolution of the Mediterranean Sea and the North African monsoon (see Cramp & O'Sullivan, 1999; Emeis & Weissert, 2009; Rohling, 1994; Rohling et al., 2015 for reviews). During orbital precession minima (Northern Hemisphere insolation maxima), the mean position of the North African monsoon front (Figure 1) migrated northwards (Rohling et al., 2002; Rossignol-Strick, 1983), resulting in so-called Green Sahara Periods (GSPs) that supported increased vegetation and potentially a more hospitable environment for hominin populations (Larrasoaña, 2021; Larrasoaña et al., 2013). Furthermore, the northward shift of the monsoon rain belt increased freshwater runoff into the Mediterranean Sea via the Nile and paleoriver systems along the wider North African margin (Rohling et al., 2002, 2015; Rossignol-Strick, 1985). High monsoon runoff increased the flux of nutrients into the Mediterranean Sea and induced water column stratification due to the formation of a buoyant low salinity surface layer. These conditions would induce deep-sea anoxia and the formation of organic-rich sapropels (Rohling et al., 2002, 2015; Rossignol-Strick et al., 1982). Furthermore, water column stratification resulted in preferential warming of the relatively fresh surface layer, a process referred to as the temperature concentration effect (Emeis et al., 2003). Not all precession minima resulted in sapropels, rather sapropels are found typically in clusters during periods when eccentricity modulation resulting in high amplitude precession cycles (Hilgen, 1991a, 1991b; Hilgen et al., 1993, 1995; Lourens et al., 1996, 2001; Rohling et al., 2015).

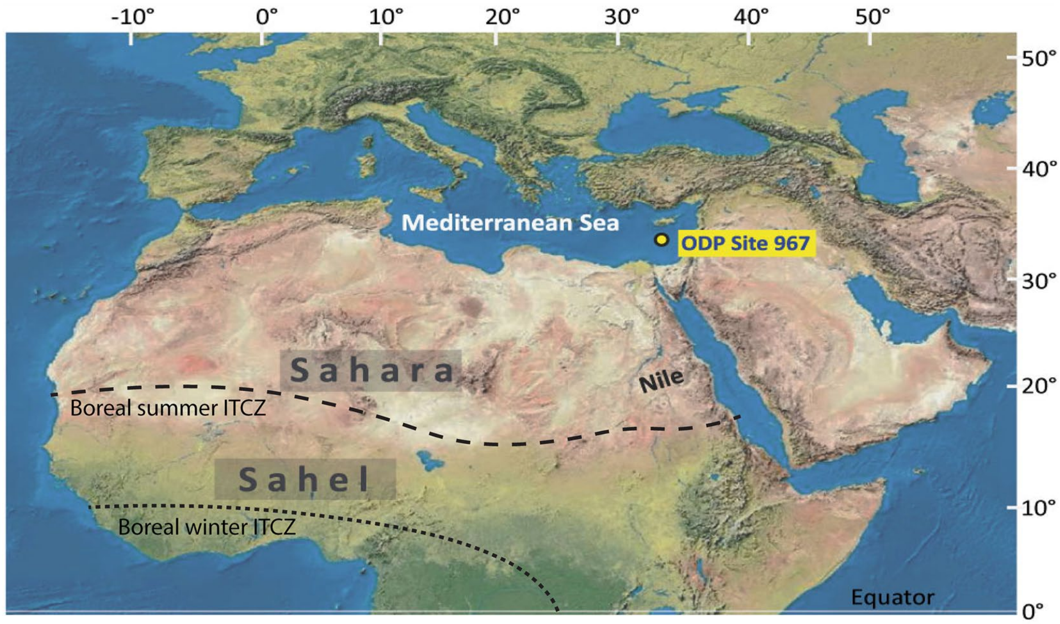

Figure 1. Map showing the Nile river and location of Ocean Drilling Program (ODP) Site 967 in the eastern Mediterranean Sea. Basemap colors indicate modern vegetated areas versus desert regions. The approximate positions of the modern boreal winter and summer Intertropical Convergence Zones (ITCZ) are show by the dotted and dashed lines, respectively (Larrasoaña et al., 2013). Monsoon rainfall over the Sahel occurs during boreal summer as the ITCZ penetrates northwards.

Monsoon runoff waters are characterized by strongly negative δ^{18}O values (Amies et al., 2019; Rohling et al., 2015, and references therein). Therefore, δ^{18}O of calcitic planktonic foraminifera tests ($\delta^{18}O_{pf}$) preserved in sapropels has the potential to provide information concerning runoff into the Mediterranean Sea and the long-term evolution of the North African monsoon (Amies et al., 2019; Emeis et al., 2003). For example, an ability to reconstruct changes in North African runoff reaching the Mediterranean Sea will enable inferences to be made concerning the strength of the monsoon and potential occurrence of GSPs during the Plio-Pleistocene, which was a key time interval for hominin evolution and dispersion (Larrasoaña, 2021; Larrasoaña et al., 2013).

We combine quantile regression (Koenker, 2005) and a Mediterranean Sea box model (Rohling, 1999; Rohling et al., 2004, 2014) to deconvolve an orbitally-tuned high-resolution $\delta^{18}O_{pf}$ record from eastern Mediterranean Ocean Drilling Program (ODP) Site 967 (Figure 1). Using box model derived sensitivities of $\delta^{18}O_{pf}$ to different forcings, we estimate the flux of North African monsoon freshwater runoff reaching the Mediterranean Sea and its associated surface water temperature concentration effect over the last 5 million years. These estimates are used to infer long-term (e.g., 400-Kyr eccentricity) orbitally-controlled changes in North African monsoon runoff.

2. Materials and Methods

Our approach is based on deconvolving long-term changes in $\delta^{18}O_{pf}$ to quantify the influence of North African monsoon runoff on the Mediterranean Sea. The deconvolution is underpinned by published records of Mediterranean $\delta^{18}O_{pf}$ and sea-level, and an established box model used to simulate changes in $\delta^{18}O_{pf}$ under different forcing scenarios. A flowchart provided in Figure 2 summarizes our proposed approach in a step-by-step fashion.

The ODP Site 967 *G. ruber* (w) δ^{18}O record of Grant et al. (2022) is adopted to represent $\delta^{18}O_{pf}$. Relative sea-level changes at Gibraltar (RSL_{Gib}) driven by variations in global mean (eustatic) sea level (ESL) were estimated from the ESL reconstruction of Rohling et al. (2021). Specifically, ESL driven change in RSL_{Gib} was obtained via the empirical relationship; $RSL_{Gib} = ESL/1.23$ estimated by Rohling et al. (2014) from an ensemble of glacial isostatic adjustment models relating ESL to depth of the Camarinal Sill (the critical location of water-exchange control for the Strait of Gibraltar). Importantly, the ESL to RSL_{Gib} conversion provides a representation of how RSL_{Gib} is expected to vary in response to ESL without associated changes in North African monsoon freshwater fluxes

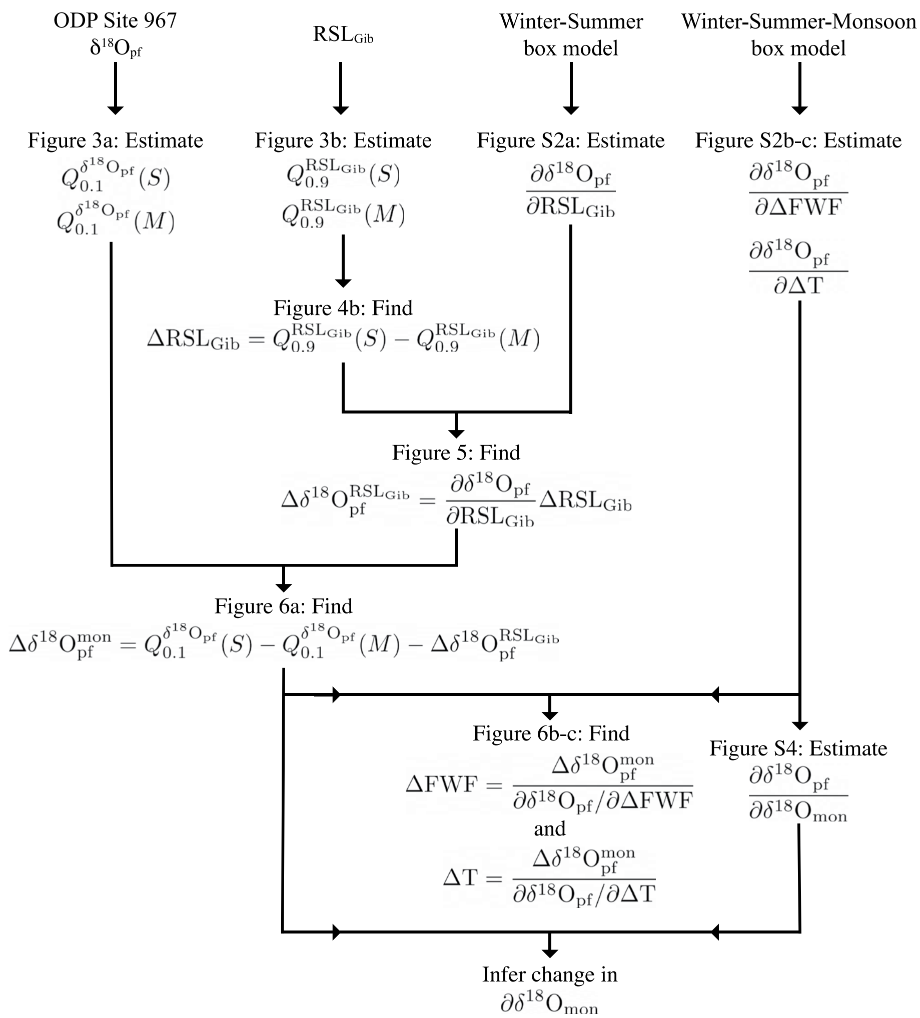

Figure 2. Flowchart of the proposed $\delta^{18}O_{pf}$ deconvolution procedure including references to the figures where each step is illustrated. Abbreviations used in the flowchart are defined at appropriate points in the text.

(FWF). Rohling et al. (2014) validated the RSL_{Gib} to ESL relationship by using it to deconvolve global deep-sea temperature since 5.3 Ma, and demonstrating that the resulting estimates were consistent with Mg/Ca-based temperatures. Following Rohling et al. (2014), we assume that RSL_{Gib} = ESL/1.23 provides a robust first-order approximation over the past 5 Myr.

The chronologies of the ODP Site 967 $\delta^{18}O_{pf}$ record of Grant et al. (2022) and the ESL record of Rohling et al. (2021) differ sufficiently that the intervals representing sapropel and marls are inconsistent. As will be shown, our deconvolution approach relies on separating records into sapropel and marl intervals, and requires that the proxies involved have a consistent age model. The Medstack composite $\delta^{18}O_{pf}$ record of Wang et al. (2010) is selected as the basis for a common chronology. Importantly, sapropel and marl age intervals are provided within the Medstack framework, facilitating our deconvolution approach. The ESL chronology of Rohling et al. (2021) is consistent with Medstack and did not require modification. Retuning the ODP Site 967 $\delta^{18}O_{pf}$ of Grant et al. (2022) to Medstack requires age adjustments of less than ±20 Kyr (Figure S1 in Supporting Information S1). To estimate variability in the North African monsoon related to 100-Kyr eccentricity cycles would require precession-scale accuracy when comparing $\delta^{18}O_{pf}$ and RSL_{Gib}. Because we cannot guarantee such age model accuracy, we focus on >400-Kyr eccentricity, which modulates both 100-Kyr eccentricity and precession. Medstack is tuned to the orbital solution of Laskar et al. (2004) and may differ slightly from more recently developed astronomical chronologies, such as CENOGRID (Westerhold et al., 2020), that are tuned to Laskar et al. (2010). However, our deconvolution is focused on long-term (>400-Kyr) variability. Therefore, systematic differences in the Medstack and CENOGRID chronologies will be unimportant unless they are on the scale of hundreds of thousands of years. Importantly, systematic differences in the Laskar et al. (2004 and 2010) orbital solutions on which the Medstack and CENOGRID chronologies are based, are minor for the age interval under consideration.

2.1. Winter-Summer Box Model

Long-term average Mediterranean Sea δ^{18}O is controlled by a broad range of parameters, which include evaporation, precipitation and runoff, Atlantic inflow, water residence time in the basin, and global ice volume. To approximate the unknown relationship between δ^{18}O and different forcings, Rohling (1999) developed a Mediterranean basin box model that included summer and winter mixed-layer separation. This box model employed parameterizations for the key forcing processes. Rohling et al. (2014) reduced many aspects of the forcing, such as summer and winter sea surface temperatures (SST_s and SST_w, respectively) to functions of RSL_{Gib}. Parameterized SST_s and SST_w (in °C) were subsequently updated by Amies et al. (2019) based on a comparison of multiple SST proxies to:

$$\mathrm{SST_s} = 22 + \frac{5.0\mathrm{RSL_{Gib}}}{120}, \tag{1}$$

and

$$\mathrm{SST_w} = 17 + \frac{3.5\mathrm{RSL_{Gib}}}{120}, \tag{2}$$

where positive values of RSL_{Gib} correspond to sea-levels above modern. *G. ruber* (w) calcification is assumed to occur in summer, and yields a $\delta^{18}O_{pf}$ according to the relationship of O'Neil (1969) with adjustments for the difference between values versus Standard Mean Ocean Water for water and versus Pee Dee Belemnite for calcite (Rohling, 1999):

$$\delta^{18}\mathrm{O_{pf}} = \frac{2.78\times10^{6}}{(\mathrm{SST_s}+273.15)^{2}} + \frac{\delta^{18}\mathrm{O_{sml}} - 30.92}{1.03092} - 3.39, \tag{3}$$

where $\delta^{18}O_{sml}$ is the δ^{18}O of the model box representing the summer mixed water layer. For compactness, we abbreviate Equation 3 to the general form; $\delta^{18}O_{pf} = f_c(\delta^{18}O, SST)$.

2.2. Winter-Summer-Monsoon Box Model

Rohling et al. (2004) extended the Mediterranean basin model to include an intermittent surface "monsoon box" to represent the influence of freshwater runoff from the North African monsoon. Such FWF have been hypothesized to be the key drivers of water column stratification in the Mediterranean during precession minima, inducing increased productivity, sapropel formation, and negative δ^{18}O anomalies (Amies et al., 2019; Emeis et al., 2003; Rohling et al., 2015; Rossignol-Strick, 1985; Rossignol-Strick et al., 1982). Based on a collection of numerical experiments aimed at simulating observed $\delta^{18}O_{pf}$ anomalies across sapropel S5, Amies et al. (2019) parameterized the depth of the box representing the monsoon-induced upper summer mixed layer (USML) as $-3.509\Delta T + 30$. For planktonic foraminifera, such as *G. ruber* (w), expected to reside in the USML:

$$\delta^{18}\mathrm{O_{pf}} = f_c\left(\delta^{18}\mathrm{O_{usml}}(\mathrm{FWF}), \mathrm{SST_s} + \Delta\mathrm{T}(\mathrm{FWF})\right), \tag{4}$$

where both $\delta^{18}O_{usml}$ and the temperature concentration effect (ΔT) depend on FWF. While ΔT is related to monsoon FWF, the form of this relationship is unknown. Therefore, Equation 3 is part of an under-identified system and it is not feasible to estimate changes in FWF (ΔFWF) and ΔT separately without additional constraints.

2.3. Box Model Sensitivities

To estimate the influence of large-scale RSL_{Gib} changes on $\delta^{18}O_{pf}$, we employ the Winter-Summer box model of Rohling (1999), with the RSL_{Gib}-based forcing parameterizations of Rohling et al. (2014), including the seasonal SST adjustments of Amies et al. (2019). In addition to determining a continuous relationship between RSL_{Gib} and $\delta^{18}O_{pf}$, we consider the sensitivity of $\delta^{18}O_{pf}$ to changes in RSL_{Gib} by determining $\partial\delta^{18}O_{pf}/\partial RSL_{Gib}$ numerically

10.1029/2023PA004677

using the Winter-Summer box model (Figure S2a in Supporting Information S1). To estimate the influence of ΔFWF and ΔT, we employ the Winter-Summer-Monsoon box model with the USML depth parameterization of Amies et al. (2019). Sensitivities $\partial\delta^{18}O_{pf}/\partial\Delta FWF$ and $\partial\delta^{18}O_{pf}/\partial\Delta T$ were estimated numerically from this model as a function of RSL_{Gib} (Figures S2b and S2c in Supporting Information S1, respectively). Sensitivity uncertainties were estimated using the Monte Carlo approach of Rohling et al. (2014), whereby for a given RSL_{Gib} an ensemble of 500 models was generated by sampling randomly the forcing parameter distributions. The resulting sensitivities are approximately Gaussian, therefore their standard error is used to represent uncertainty at a given RSL_{Gib}. Changes in monsoon FWF represented by ΔFWF are scaled according to model estimates of the preindustrial annual Nile river runoff (Colleoni et al., 2015). Therefore, $\Delta FWF = 1$ represents a monsoon FWF equal to the preindustrial annual Nile river runoff, $\Delta FWF = 2$ corresponds to a monsoon FWF of twice the preindustrial annual Nile river runoff, etc.

2.4. Deconvolution of North African Freshwater Flux

As discussed, freshening of surface waters due to enhanced ΔFWF is hypothesized to have induced water column stratification. During these intervals, negative $\delta^{18}O_{pf}$ anomalies reflect both isotopically depleted surface waters and temperature concentration effects (Equation 4). Therefore, estimating the magnitude of the $\delta^{18}O_{pf}$ anomaly combined with box model estimates of $\delta^{18}O_{pf}$ sensitivities provides an approach to assess ΔFWF and ΔT in combination.

Estimation of $\delta^{18}O_{pf}$ anomalies in sapropel intervals requires interpolating non-sapropelic $\delta^{18}O_{pf}$ across the sapropel in a physically meaningful way. For example, within the sapropel interval $\delta^{18}O_{pf}$ may have been influenced by a number of factors, such as insolation driven changes in RSL_{Gib} and SST_s, that are not related directly to ΔFWF and ΔT. Therefore, given the $\delta^{18}O_{pf}$ observations, it is necessary to estimate $\delta^{18}O_{pf}$ across the sapropel interval in a form consistent with ΔFWF and ΔT being zero. The difference between this estimate and the observations corresponds to the monsoon-related $\delta^{18}O_{pf}$ anomaly ($\Delta\delta^{18}O_{pf}^{mon}$) resulting from FWF and temperature concentration effects. The required ΔFWF and ΔT to obtain such an anomaly can then be estimated via $\partial\delta^{18}O_{pf}/\partial\Delta FWF$ and $\partial\delta^{18}O_{pf}/\partial\Delta T$ sensitivities obtained from the Winter-Summer-Monsoon box model (Figure 2).

As explained above, our aim is to reconstruct long-term (400-Kyr eccentricity and longer) variations in ΔFWF and ΔT. Therefore, while not all sapropel intervals may conform purely with a North African monsoon FWF forcing scenario (Rohling et al., 2015), it is considered that this will be the primary process driving long-term changes in sapropel $\delta^{18}O_{pf}$ anomalies. To assess long-term trends in $\delta^{18}O_{pf}$, both within sapropel peaks and in the portions of marls with low $\delta^{18}O_{pf}$ preceding and following sapropels, we employ quantile regression (Koenker, 2005). Quantile regression provides estimates of conditional quantiles, in contrast to traditional regression which estimates the conditional mean of a dependent variable. Quantile regression estimates are obtained by minimizing the difference between observed quantiles and those predicted using a parametric regression function. We utilize a smoothing cubic spline to obtain quantile regression estimates, with the degrees of freedom (dof) of the spline controlling its smoothness. Quantile spline fits were obtained using the *statsmodel* package (Seabold & Perktold, 2010). The uncertainty associated with a quantile spline fit at given age point is Gaussian (Koenker, 2005). Therefore, a 95% confidence interval can be obtained at each age point as ± 1.96SE, where SE is the standard error of the fit at that point as provided by the *statsmodel* algorithm. Analytical uncertainties on each $\delta^{18}O_{pf}$ point are assumed to be negligible and are therefore not considered in the quantile spline fitting procedure.

To represent the evolution of sapropel minimum $\delta^{18}O_{pf}$ values, a smoothing cubic spline (dof = 50) was fit to the 0.1 quantile of ODP Site 967 $\delta^{18}O_{pf}$ observations within sapropel intervals ($Q_{0.1}^{\delta^{18}O_{pf}}(S)$). Correspondingly, a second cubic spline (dof = 50) was fit to the 0.1 quantile of the $\delta^{18}O_{pf}$ in the marl intervals ($Q_{0.1}^{\delta^{18}O_{pf}}(M)$, Figure 3a). The spline dof was selected based on its numerically-estimated frequency response (Figure S3 in Supporting Information S1), which includes the 400-Kyr eccentricity cycle that modulates the amplitude of precession and sapropel formation. As discussed earlier, the frequency response of the spline means that while the chronologies of the employed proxy records must be internally consistent, systematic differences between available age models (e.g., Medstack vs. CENOGRID) will be unimportant.

The fitted splines provide an estimate of the difference in $\delta^{18}O_{pf}$ minima between marls and sapropels; however, they do not consider the effect of non-monsoon dependent forcings, such as RSL_{Gib}, that influence $\delta^{18}O_{pf}$ in sapropels independently of ΔFWF and ΔT. To assess this influence, cubic splines (dof = 50) were fitted to the

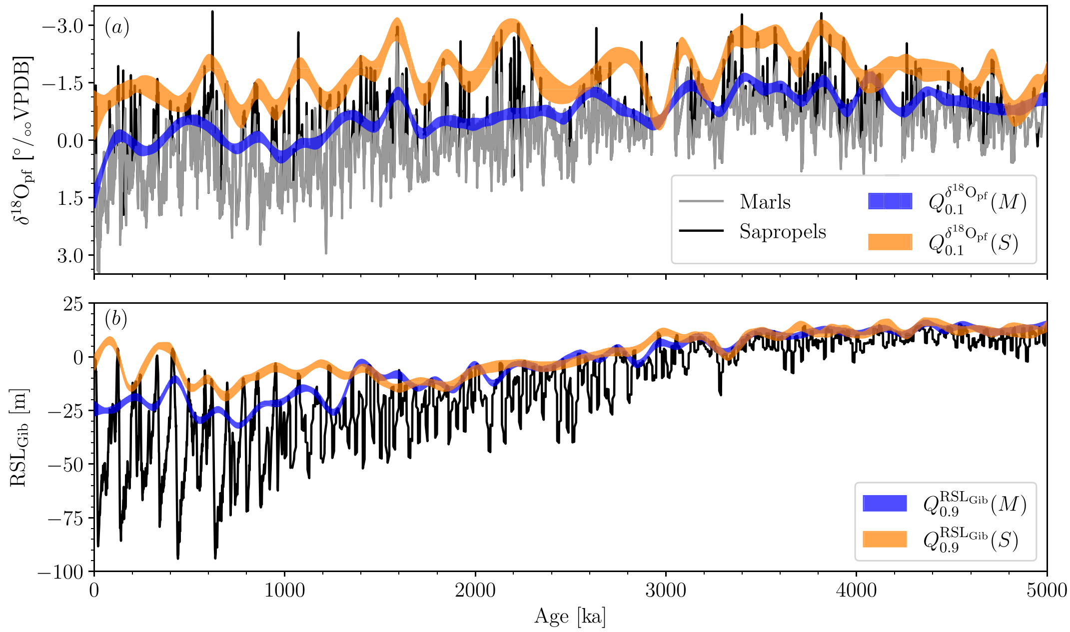

Figure 3. (a) Quantile regression of the Ocean Drilling Program Site 967 $\delta^{18}O_{pf}$ record. Marl and sapropel samples are shown in gray and black, respectively. Blue and orange represent the 0.1 quantiles for the marls ($Q_{0.1}^{\delta^{18}O_{pf}}(M)$) and sapropels ($Q_{0.1}^{\delta^{18}O_{pf}}(S)$), respectively, with the width of the bands corresponding to their 95% confidence intervals. (b) Quantile regression of the RSL_{Gib} sea-level reconstruction. Blue and orange represent the 0.9 quantiles for the marls ($Q_{0.9}^{RSL_{Gib}}(M)$) and sapropels ($Q_{0.9}^{RSL_{Gib}}(S)$), respectively, with the width of the bands corresponding to their 95% confidence interval. Negative RSL_{Gib} values indicate sea-levels below modern.

0.9 quantiles of RSL_{Gib} for the sapropel and marl intervals ($Q_{0.9}^{RSL_{Gib}}(S)$, and $Q_{0.9}^{RSL_{Gib}}(M)$, respectively, Figure 3b). The mean ($\overline{RSL_{Gib}}$) and difference (ΔRSL_{Gib}) in the RSL_{Gib} quantiles can be expressed as:

$$\overline{RSL_{Gib}} = \frac{Q_{0.9}^{RSL_{Gib}}(S) + Q_{0.9}^{RSL_{Gib}}(M)}{2}, \tag{5}$$

and

$$\Delta RSL_{Gib} = Q_{0.9}^{RSL_{Gib}}(S) - Q_{0.9}^{RSL_{Gib}}(M). \tag{6}$$

Figure 4 demonstrates that ΔRSL_{Gib} increased markedly with the onset of the Mid-Pleistocene Transition (~1.2 Ma) when the contrast between glacials characterized by large ice sheets and interglacials increased (Chalk et al., 2017).

As discussed in Section 2.1, the Winter-Summer box model parameterizes forcing as a function of RSL_{Gib} (Rohling et al., 2014). Therefore box-model derived $\partial\delta^{18}O_{pf}/\partial RSL_{Gib}$ sensitivity provides an estimate of the $\delta^{18}O_{pf}$ contribution within sapropels that is not related to ΔFWF and ΔT (Figure S2a in Supporting Information S1). Once this RSL_{Gib}-related contribution is accounted for, the difference in $\delta^{18}O_{pf}$ 0.1 quantiles between the sapropel and marl intervals yields an estimate of $\Delta\delta^{18}O_{pf}^{mon}$ (Figure 2). Specifically, within a sapropel the anomaly due to changes in forcing parameterized as a function of RSL_{Gib} is given by (Figures 2 and 5):

$$\Delta\delta^{18}O_{pf}^{RSL_{Gib}} = \Delta RSL_{Gib}\frac{\partial\delta^{18}O_{pf}}{\partial RSL_{Gib}}, \tag{7}$$

where the value of $\partial\delta^{18}O_{pf}/\partial RSL_{Gib}$ (Figure S2a in Supporting Information S1) is set according to $\overline{RSL_{Gib}}$ (Figure 4). The final anomaly is then (Figures 2 and 6a):

$$\Delta\delta^{18}O_{pf}^{mon} = Q_{0.1}^{\delta^{18}O_{pf}}(S) - Q_{0.1}^{\delta^{18}O_{pf}}(M) - \Delta\delta^{18}O_{pf}^{RSL_{Gib}}. \tag{8}$$

10.1029/2023PA004677

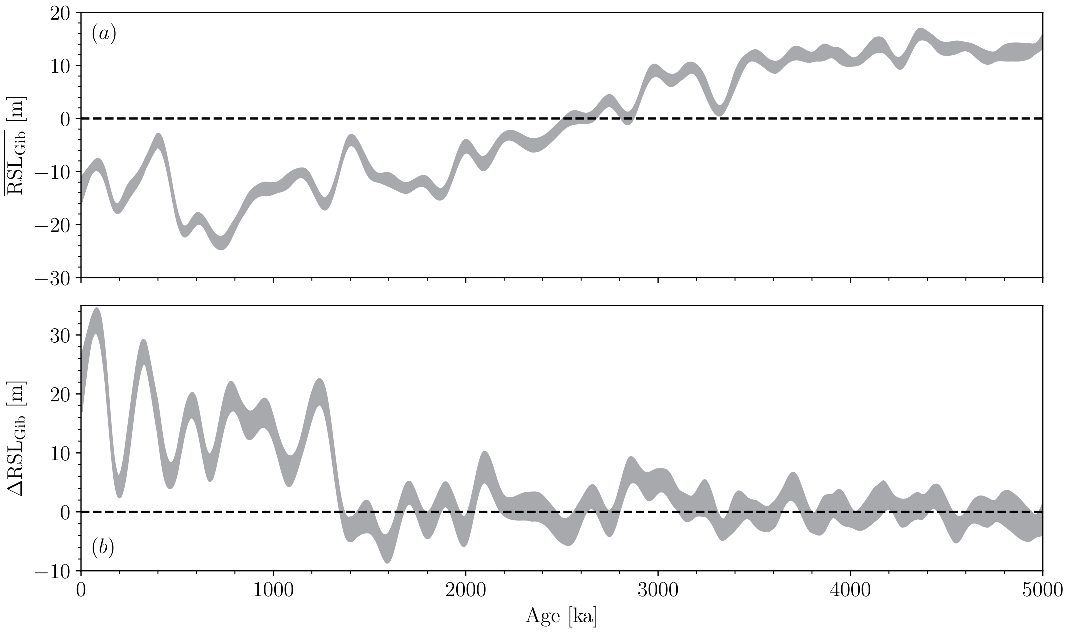

Figure 4. (a) Estimated mean $\mathrm{RSL_{Gib}}$ through sapropel intervals based on the mean of $Q_{0.9}^{\mathrm{RSL_{Gib}}}(S)$ and $Q_{0.9}^{\mathrm{RSL_{Gib}}}(M)$. The width of the band corresponds to the 95% confidence interval. (b) Estimated difference in $\mathrm{RSL_{Gib}}$ between marl and sapropel intervals based on the difference between $Q_{0.9}^{\mathrm{RSL}}(S)$ and $Q_{0.9}^{\mathrm{RSL}}(M)$. The width of the band corresponds to the 95% confidence interval.

Estimates of $\partial\delta^{18}\mathrm{O_{pf}}/\partial\Delta\mathrm{FWF}$ and $\partial\delta^{18}\mathrm{O_{pf}}/\partial\Delta\mathrm{T}$ enable estimation of the maximum ΔFWF or ΔT that could be responsible for the estimated $\Delta\delta^{18}\mathrm{O_{pf}^{mon}}$ sapropel anomalies. As shown in Figures S2b and S2c in Supporting Information S1, $\partial\delta^{18}\mathrm{O_{pf}}/\partial\Delta\mathrm{FWF}$ and $\partial\delta^{18}\mathrm{O_{pf}}/\partial\Delta\mathrm{T}$ are not independent of $\mathrm{RSL_{Gib}}$. Therefore, $\partial\delta^{18}\mathrm{O_{pf}}/\partial\Delta\mathrm{FWF}$ and $\partial\delta^{18}\mathrm{O_{pf}}/\partial\Delta\mathrm{T}$ values are selected as a function of $\overline{\mathrm{RSL_{Gib}}}$.

As shown in Figure 2, our proposed deconvolution only requires basic arithmetic operations (addition, subtraction, division, and multiplication). Therefore, the Gaussian distributed uncertainties associated with the quantile spline fits and box-model sensitivities were propagated using the variance formula (Taylor, 1997):

$$\delta q = \sqrt{\left(\frac{\partial q}{\partial x}\delta x\right)^2 + \cdots + \left(\frac{\partial q}{\partial z}\delta z\right)^2} \tag{9}$$

where q is a function of several variables $x, \ldots, z$ with uncertainties $\delta x, \ldots, \delta z$. Estimated standard errors were converted to 95% confidence intervals via multiplication with a factor of ±1.96.

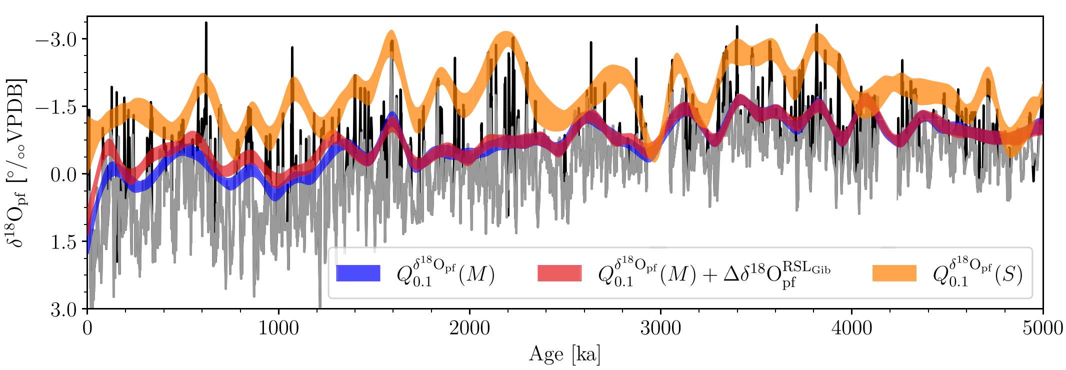

Figure 5. As in Figure 3a, with the addition of the estimated $\mathrm{RSL_{Gib}}$ forced contribution to the marl 0.1 $\delta^{18}\mathrm{O_{pf}}$ quantile (red).

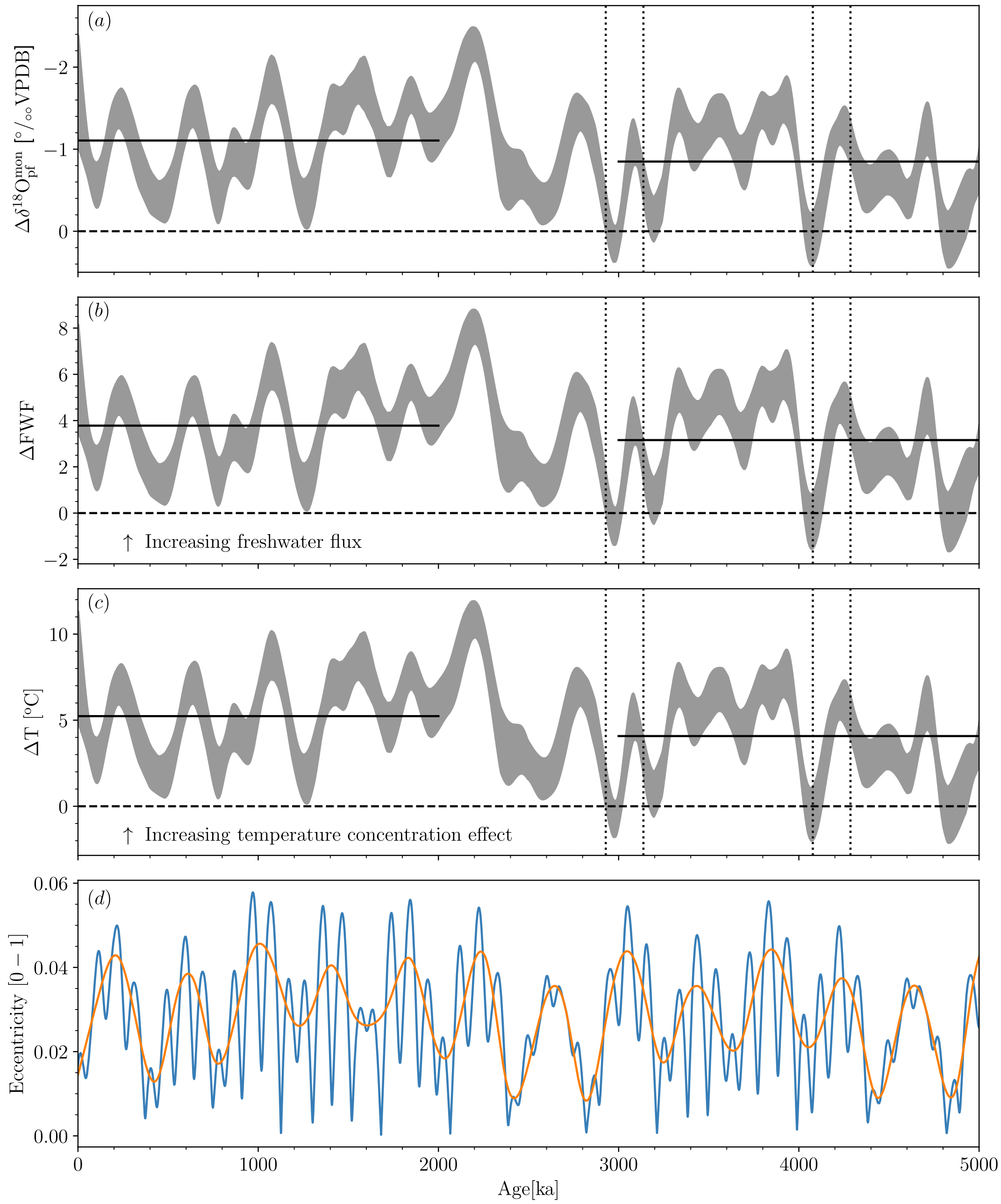

Figure 6. (a) Estimated $\Delta\delta^{1}8O_{pf}^{mon}$ anomaly due to (b) monsoon freshwater fluxes (FWF) and (c) temperature concentration effects. Shading represents the 95% confidence interval. Dotted lines show the region of the reconstruction where the quantile regression cubic splines may have been unduly influenced by gaps in the Ocean Drilling Program Site 967 $\delta^{18}O_{pf}$ record (Figure 3a). Solid black lines represent long-term means between 3–5 and 0–2 Ma. (d) Orbital eccentricity (blue) from the astronomical solution of Laskar et al. (2004). A 0.5 quantile regression with a dof = 50 smoothing cubic spline is shown in orange to emphasize the 400-Kyr eccentricity cycle.

3. Results and Discussion

Our approach provides an estimate of the $\Delta\delta^{18}O_{pf}$ anomaly due to monsoon-related freshwater runoff from the North African margin and Nile river (Figure 6a). Based on $\partial\delta^{18}O_{pf}/\partial\Delta FWF$ and $\partial\delta^{18}O_{pf}/\partial\Delta T$ sensitivities (Figures S2b and S2c in Supporting Information S1, respectively), estimated anomalies can be converted into ΔFWF and ΔT anomalies (Figures 6b and 6c, respectively). As highlighted in Equation 4, because $\Delta\delta^{18}O_{pf}^{mon}$ is based on a single species, it is not feasible to estimate ΔFWF and ΔT simultaneously without additional constraints.

10.1029/2023PA004677

Therefore, the ΔFWF and ΔT anomalies are not independent of each other (the temperature concentration effect responsible for ΔT is a result of water column stratification induced by ΔFWF). The anomaly estimates, thus, represent the ΔFWF and ΔT required individually, not in combination, to explain $\Delta\delta^{18}O_{pf}^{mon}$. At 5 Ma, for example, $\Delta\delta^{18}O_{pf}^{mon} \approx -0.6$‰ corresponding to either ΔFWF ≈ 2 or ΔT ≈ 2.5°C. These anomalies must be interpreted as end-member scenarios, and the actual ΔFWF and ΔT anomalies will be some, potentially nonlinear, mixture of those end-members. Therefore, ΔFWF and ΔT should be interpreted as an indicative range of potential anomalies rather than a quantitative estimate of actual anomalies.

Within estimated uncertainties, $\Delta\delta^{18}O_{pf}^{mon}$ ranges from ∼0‰, corresponding to minimal addition of monsoon freshwater in the sapropel intervals, through to an extreme of ∼−2‰. Longer period variability in $\Delta\delta^{18}O_{pf}^{mon}$ follows the 400-Kyr cycle in eccentricity (Figure 6d). This is to be expected given that the 400-Kyr eccentricity cycle modulates the amplitude of the 100-Kyr eccentricity cycle, which in-turn modulates precession and therefore insolation (Laskar et al., 2004). While such a pattern cannot be used to infer the existence of specific GSPs, it indicates that monsoon conditions conducive to GSPs occurred persistently over the last 5 Ma during peaks in the 400-Kyr eccentricity cycle.

Amies et al. (2019) employed a multi-species reconstruction to estimate that the *G. ruber* (w) $\delta^{18}O_{pf}$ anomaly associated with sapropel S5 (∼128.3–121.5 ka, Grant et al., 2016) was ∼−2‰ at ODP Site 967. Based on high-resolution mean annual SST (alkenone unsaturation index, $U_{37}^{K'}$ (Marino et al., 2007; Rohling et al., 2002)) and summer SST estimates (carbonate clumped isotope thermometry, Δ_{47} (Rodríguez-Sanz et al., 2017)), Amies et al. (2019) were able to parameterize the temperature concentration effect through S5 and make an independent estimate of ΔFWF. Specifically, based on an inverse box model and data from a collection of Mediterranean sites, Amies et al. (2019) attributed the S5 $\delta^{18}O_{pf}$ anomaly to an ≤8.8 times increase in Nile FWF (relative to modern pre-Aswan discharge) and a temperature concentration effect of ≤5.7°C. These values are broadly consistent with our estimated $\Delta\delta^{18}O_{pf}^{mon}$ if they are considered separately (i.e., an ≤8.8 times increase in Nile FWF, or a temperature concentration effect of ≤5.7°C), but not in combination. For example, based on the sensitivities in Figures S2b and S2c in Supporting Information S1, a ΔFWF of 8.8 and ΔT of 5.7°C would yield an anomaly of ∼−3.5‰. Importantly, without high-quality SST estimates through the ODP Site 967 record, construction of independent estimates of temperature concentration is not feasible. For example, existing Mediterranean SST records for the Plio-Pleistocene (Herbert et al., 2015) have 95% confidence intervals of ±2.9°C (Müller et al., 1998), which is greater than the amplitude of the estimated ODP Site 967 long eccentricity temperature concentration cycles (Figure 6c). This demonstrates the challenges associated with making long duration quantitative reconstructions of past monsoon activity when the physical relationship between ΔFWF and ΔT is understood poorly.

At ∼2.6 Ma, there is a shift in $\Delta\delta^{18}O_{pf}^{mon}$ toward more negative values and larger amplitude cycles, implying potentially larger ΔFWF and/or ΔT that cannot be explained by eccentricity changes alone (Figure 6). The shift in the mean was assessed by estimating long-term $\Delta\delta^{18}O_{pf}^{mon}$ averages (before 3 Ma and after 2 Ma) and has a magnitude of ∼−0.25‰. Such a shift in the mean $\Delta\delta^{18}O_{pf}^{mon}$ is opposite to previously hypothesized forcing mechanisms inferred from the analysis of proxy reconstructions and climate model simulations. For example, based on a suite of preindustrial and Pliocene simulations, Colleoni et al. (2015) inferred that freshwater flux into the Mediterranean Sea from the North African margin and Nile river was ∼40% higher during the Pliocene. Their simulations did not consider monsoon anomalies in sapropels specifically, but their work indicates a more active hydrological system during the Pliocene. Based on high-resolution elemental ratios and $\delta^{18}O_{pf}$ records, it has been hypothesized that at 3.2 Ma, when the gradual evolution to modern North African aridity commenced, monsoon-related freshwater flux remained relatively constant (Grant et al., 2022).

On the basis of atmospheric general circulation models, Colleoni et al. (2015) hypothesized that the pattern of freshwater runoff around the Mediterranean changed across the Plio-Pleistocene transition. They concluded that evolution of atmospheric circulation over the Mediterranean began at ∼3 Ma and long-range teleconnections achieved their present-day configuration by ∼1.8 Ma. As mentioned above, Pliocene simulations by Colleoni et al. (2015) revealed a more active hydrological network in North Africa, a feature interpreted to result from the descending branch of the Hadley cell reaching further north. These simulations highlight that although the magnitude of freshwater flux reaching the Mediterranean from North Africa was higher during the Pliocene, the configuration of the hydrological network was also different. Given the available observational (Grant et al., 2022) and modeling (Colleoni et al., 2015) constraints, it is apparent that a shift to more negative $\Delta\delta^{18}O_{pf}^{mon}$

values and larger amplitude cycles at ∼2.6 Ma cannot be attributed unequivocally to a larger and more variable freshwater flux in the Pleistocene.

Using the CLIMBER-2 Earth-system model, de Boer et al. (2021) investigated the impact of the African monsoon on the Mediterranean between 3.2 and 2.3 Ma. Based on simulated changes in the North African hydrological network combined with proxy records for continental runoff, they estimated that prior to ∼2.8 Ma the contribution of runoff originating from the Sahara region was dominant over runoff originating from the Sahel (Figure 1). After ∼2.8 Ma and the onset of global cooling and inception of North Hemisphere glaciations, a scenario with approximately equal runoff contributions from the Sahara and Sahel regions is most consistent with proxy information. As highlighted by Amies et al. (2019) and Rohling et al. (2015), the δ^{18}O of freshwater during monsoon maxima in areas of North Africa that are currently covered by the Saharan desert is between −8 and −12‰. Therefore, the Winter-Summer-Monsoon box model was used to determine the sensitivity; $\partial\delta^{18}O_{pf}/\partial\delta^{18}O_{mon}$, where $\delta^{18}O_{mon}$ is the δ^{18}O composition of the monsoon FWF (Figure 2). Based on the $\Delta\delta^{18}O_{pf}^{mon}$ anomalies in Figure 6a, $\partial\delta^{18}O_{pf}/\partial\delta^{18}O_{mon}$ was estimated for ΔFWF = 4 (Figure S4 in Supporting Information S1). The sensitivity of $\delta^{18}O_{pf}$ to changes in $\delta^{18}O_{mon}$ implies that the observed change in $\Delta\delta^{18}O_{pf}^{mon}$ can be explained readily by a shift in δ^{18}O of monsoon FWF of ∼−3‰ within the expected −8 and −12‰ interval. While this hypothesis will require more detailed investigation in future studies, it indicates the magnitude of the influence FWF δ^{18}O composition may have Mediterranean $\delta^{18}O_{pf}$.

4. Conclusions

Through a combination of high-resolution proxy data, box model derived sensitivities, and quantile regression, we have estimated $\delta^{18}O_{pf}$ anomalies associated with North African monsoon runoff into the Mediterranean Sea. Based on these anomalies, estimated North African monsoon activity has followed eccentricity modulation of precession throughout the last 5 Ma, which is a pattern consistent with known orbital drivers of sapropel formation. During peaks in the 400-Kyr eccentricity cycle, $\Delta\delta^{18}O_{pf}^{mon}$ anomalies are consistent with a FWF increase corresponding to ∼7 times the preindustrial annual output of the Nile river, or a temperature concentration effect of ∼8°C. Such a long-term pattern in monsoon FWF variability, and thus Mediterranean Sea stratification, is consistent with the occurrence of sapropels in the Mediterranean since the Miocene (Hilgen et al., 1995).

A negative shift in the background value of $\Delta\delta^{18}O_{pf}^{mon}$ anomalies occurs around the onset of Northern Hemisphere glaciations. Based on box model sensitivities, this shift corresponds to a change in $\delta^{18}O_{mon}$ of ∼−3‰. Given uncertainties in $\delta^{18}O_{mon}$ through time (Amies et al., 2019; Rohling et al., 2015) and Earth-system model results indicating a change in monsoon freshwater source area coincident with the inception of Northern Hemisphere ice sheets (de Boer et al., 2021), we hypothesize that the reconstructed shift may be attributed to a change in the source area and/or composition of FWF entering the Mediterranean Sea. We have demonstrated that this hypothesis is feasible and it should be tested in the future.

Finally, based on the estimated monsoon FWF reaching the Mediterranean Sea over the last 5 Ma, the potential for conditions conducive to the occurrence of GSPs is clear. Given that monsoon FWF is modulated strongly by eccentricity, this provides an indication during which precession minima GSPs may have occurred.

Data Availability Statement

Jupyter notebooks, associated Python and Julia code, and data files to recreate the calculations presented in this work are available at Heslop (2023).

Acknowledgments
This work was supported by the Australian Research Council Grants FL120100050 and DP200101157. The authors are grateful to the Editor, Associate Editor, and three reviewers for their constructive comments that helped to improve the final manuscript. Open access publishing facilitated by Australian National University, as part of the Wiley - Australian National University agreement via the Council of Australian University Librarians.

References

Amies, J. D., Rohling, E. J., Grant, K. M., Rodriquez-Sanz, L., & Marino, G. (2019). Quantification of African monsoon runoff during last interglacial sapropel S5. *Paleoceanography and Paleoclimatology*, *34*(8), 1487–1516. https://doi.org/10.1029/2019PA003652

Chalk, T. B., Hain, M. P., Foster, G. L., Rohling, E. J., Sexton, P. F., Badger, M. P. S., et al. (2017). Causes of ice age intensification across the Mid-Pleistocene Transition. *Proceedings of the National Academy of Sciences*, *114*(50), 13114–13119. https://doi.org/10.1073/pnas.1702143114

Colleoni, F., Cherchi, A., Masina, S., & Brierley, C. M. (2015). Impact of global SST gradients on the Mediterranean runoff changes across the Plio-Pleistocene transition. *Paleoceanography*, *30*(6), 751–767. https://doi.org/10.1002/2015PA002780

Cramp, A., & O'Sullivan, G. (1999). Neogene sapropels in the Mediterranean: A review. *Marine Geology*, *153*(1–4), 11–28. https://doi.org/10.1016/S0025-3227(98)00092-9 de Boer, B., Peters, M., & Lourens, L. J. (2021). The transient impact of the African monsoon on Plio-Pleistocene Mediterranean sediments. *Climate of the Past*, *17*(1), 331–344. https://doi.org/10.5194/cp-17-331-2021

Emeis, K.-C., Schulz, H., Struck, U., Rossignol-Strick, M., Erlenkeuser, H., Howell, M. W., et al. (2003). Eastern Mediterranean surface water temperatures and $\delta^{18}O$ composition during deposition of sapropels in the late Quaternary. *Paleoceanography*, *18*(1), 1005. https://doi.org/10.1029/2000PA000617

Emeis, K.-C., & Weissert, H. (2009). Tethyan-Mediterranean organic carbon-rich sediments from Mesozoic black shales to sapropels. *Sedimentology*, *56*(1), 247–266. https://doi.org/10.1111/j.1365-3091.2008.01026.x

Grant, K. M., Amarathunga, U., Amies, J. D., Hu, P.-X., Qian, Y., Penny, T., et al. (2022). Organic carbon burial in Mediterranean sapropels intensified during Green Sahara Periods since 3.2 Myr ago. *Communications Earth & Environment*, *3*(1), 11. https://doi.org/10.1038/s43247-021-00339-9

Grant, K. M., Grimm, R., Mikolajewicz, U., Marino, G., Ziegler, M., & Rohling, E. J. (2016). The timing of Mediterranean sapropel deposition relative to insolation, sea-level and African monsoon changes. *Quaternary Science Reviews*, *140*, 125–141. https://doi.org/10.1016/j.quascirev.2016.03.026

Herbert, T. D., Ng, G., & Peterson, L. C. (2015). Evolution of Mediterranean sea surface temperatures 3.5-1.5 Ma: Regional and hemispheric influences. *Earth and Planetary Science Letters*, *409*, 307–318. https://doi.org/10.1016/j.epsl.2014.10.006

Heslop, D. (2023). dave-heslop74/ODP-Site-967-Models: v1.0.0 (v1.0.0) [Software]. Zenodo. https://doi.org/10.5281/zenodo.8267837

Hilgen, F. J. (1991a). Astronomical calibration of Gauss to Matuyama sapropels in the Mediterranean and implication for the geomagnetic polarity time scale. *Earth and Planetary Science Letters*, *104*(2–4), 226–244. https://doi.org/10.1016/0012-821X(91)90206-W

Hilgen, F. J. (1991b). Extension of the astronomically calibrated (polarity) timescale to the Miocene/Pliocene boundary. *Earth and Planetary Science Letters*, *107*(2), 349–368. https://doi.org/10.1016/0012-821X(91)90082-S

Hilgen, F. J., Krijgsman, W., Langereis, C. G., Lourens, L. J., Santarelli, A., & Zachariasse, W. J. (1995). Extending the astronomical (polarity) time scale into the Miocene. *Earth and Planetary Science Letters*, *136*(3–4), 495–510. https://doi.org/10.1016/0012-821X(95)00207-S

Hilgen, F. J., Lourens, L. J., Berger, A., & Loutre, M. F. (1993). Evaluation of the astronomically calibrated time scale for the late Pliocene and earliest Pleistocene. *Paleoceanography*, *8*(5), 549–565. https://doi.org/10.1029/93PA01248

Koenker, R. (2005). *Quantile regression* (p. 146). Cambridge University Press.

Larrasoaña, J. C. (2021). A review of West African monsoon penetration during Green Sahara periods; implications for human evolution and dispersals over the last three million years. *Oxford Open Climate Change*, *1*, kgab011. https://doi.org/10.1093/oxfclm/kgab011

Larrasoaña, J. C., Roberts, A. P., & Rohling, E. J. (2013). Dynamics of Green Sahara periods and their role in hominin evolution. *PLoS One*, *8*(10), e76514. https://doi.org/10.1371/journal.pone.0076514

Laskar, J., Fienga, A., Gastineau, M., & Manche, H. (2010). La2010: A new orbital solution for the long-term motion of the Earth. *Astronomy & Astrophysics*, *532*, A89. https://doi.org/10.1051/0004-6361/201116836

Laskar, J., Robutel, P., Joutel, F., Gastineau, M., Correia, A. C. M., & Levrard, B. (2004). A long-term numerical solution for the insolation quantities of the Earth. *Astronomy & Astrophysics*, *428*(1), 261–285. https://doi.org/10.1051/0004-6361:20041335

Lourens, L. J., Antonarakou, A., Hilgen, F. J., Van Hoof, A. A. M., Vergnaud-Grazzini, C., & Zachariasse, W. J. (1996). Evaluation of the Plio-Pleistocene astronomical time-scale. *Paleoceanography*, *11*(4), 391–413. https://doi.org/10.1029/96PA01125

Lourens, L. J., Wehausen, R., & Brumsack, H. J. (2001). Geological constraints on tidal dissipation and dynamical ellipticity of the Earth over the past three million years. *Nature*, *409*(6823), 1029–1033. https://doi.org/10.1038/35059062

Marino, G., Rohling, E. J., Rijpstra, W. I. C., Sangiorgi, F., Schouten, S., & Sinninghe Damsté, J. S. (2007). Aegean Sea as a driver of hydrographic and ecological changes in the eastern Mediterranean. *Geology*, *35*(8), 675–678. https://doi.org/10.1130/G23831A.1

Müller, P. J., Kirst, G., Ruhland, G., von Storch, I., & Rosell-Melé, A. (1998). Calibration of the alkenone paleotemperature index $U_{37}^{K'}$ based on core-tops from the eastern South Atlantic and the global ocean (60°N-60°S). *Geochimica et Cosmochimica Acta*, *62*(10), 1757–1772. https://doi.org/10.1016/S0016-7037(98)00097-0

O'Neil, J. R. (1969). Oxygen isotope fractionation on divalent metal carbonates. *Journal of Chemical Physics*, *51*(12), 5547–5558. https://doi.org/10.1063/1.1671982

Rodríguez-Sanz, L., Bernasconi, S. M., Marino, G., Heslop, D., Müller, I. A., Fernandez, A., et al. (2017). Penultimate deglacial warming across the Mediterranean Sea revealed by clumped isotopes in foraminifera. *Scientific Reports*, *7*(1), 16572. https://doi.org/10.1038/s41598-017-16528-6

Rohling, E. J. (1994). Review and new aspects concerning the formation of eastern Mediterranean sapropels. *Marine Geology*, *122*(1–2), 1–28. https://doi.org/10.1016/0025-3227(94)90202-X

Rohling, E. J. (1999). Environmental control on Mediterranean salinity and $\delta^{18}O$. *Paleoceanography*, *14*(6), 706–715. https://doi.org/10.1029/1999PA900042

Rohling, E. J., Cane, T. R., Cooke, S., Sprovieri, M., Bouloubassi, I., Emeis, K.-C., et al. (2002). African monsoon variability during the previous interglacial maximum. *Earth and Planetary Science Letters*, *202*(1), 61–75. https://doi.org/10.1016/S0012-821X(02)00775-6

Rohling, E. J., Foster, G. L., Grant, K. M., Marino, G., Roberts, A. P., Tamisiea, M. E., & Williams, F. (2014). Sea-level and deep-sea-temperature variability over the past 5.3 million years. *Nature*, *508*(7497), 477–482. https://doi.org/10.1038/nature13230

Rohling, E. J., Marino, G., & Grant, K. M. (2015). Mediterranean climate and oceanography, and the periodic development of anoxic events (sapropels). *Earth-Science Reviews*, *143*, 62–97. https://doi.org/10.1016/j.earscirev.2015.01.008

Rohling, E. J., Sprovieri, M., Cane, T., Casford, J. S. L., Cooke, S., Bouloubassi, I., et al. (2004). Reconstructing past planktic foraminiferal habitats using stable isotope data: A case history for Mediterranean sapropel S5. *Marine Micropaleontology*, *50*(1–2), 89–123. https://doi.org/10.1016/S0377-8398(03)00068-9

Rohling, E. J., Yu, J., Heslop, D., Foster, G. L., Opdyke, B., & Roberts, A. P. (2021). Sea-level and deep-sea temperature reconstructions suggest quasi-stable states and critical transitions over the past 40 million years. *Science Advances*, *7*(26), eabf5326. https://doi.org/10.1126/sciadv.abf5326

Rossignol-Strick, M. (1983). African monsoons, an immediate climate response to orbital insolation. *Nature*, *304*(5921), 46–49. https://doi.org/10.1038/304046a0

Rossignol-Strick, M. (1985). Mediterranean Quaternary sapropels, an immediate response of the African monsoon to variation in insolation. *Palaeogeography, Palaeoclimatology, Palaeoecology*, *49*(3–4), 237–263. https://doi.org/10.1016/0031-0182(85)90056-2

Rossignol-Strick, M., Nesteroff, W., Olive, P., & Vergnaud-Grazzini, C. (1982). After the deluge: Mediterranean stagnation and sapropel formation. *Nature*, *295*(5845), 105–110. https://doi.org/10.1038/295105a0

Seabold, S., & Perktold, J. (2010). Statsmodels: Econometric and statistical modeling with python. In *9th Python in science conference*.

Taylor, J. R. (1997). *An introduction to error analysis: The study of uncertainties in physical measurements* (p. 327). University Science Books.

Wang, P., Tian, J., & Lourens, L. J. (2010). Obscuring of long eccentricity cyclicity in Pleistocene oceanic carbon isotope records. *Earth and Planetary Science Letters*, *290*(3–4), 319–330. https://doi.org/10.1016/j.epsl.2009.12.028

Westerhold, T., Marwan, N., Drury, A. J., Liebrand, D., Agnini, C., Anagnostou, E., et al. (2020). An astronomically dated record of Earth's climate and its predictability over the last 66 million years. *Science*, *369*(6509), 1383–1387. https://doi.org/10.1126/science.aba6853